Precise study of asymptotic physics with subradiant ultracold molecules

B. H. McGuyer,[1] M. McDonald,[1] G. Z. Iwata,[1] M. G. Tarallo,[1] W. Skomorowski,[2, *] R. Moszynski,[2] and T. Zelevinsky[1]

[1]*Department of Physics, Columbia University, 538 West 120th Street, New York, NY 10027-5255, USA*
[2]*Quantum Chemistry Laboratory, Department of Chemistry,*
University of Warsaw, Pasteura 1, 02-093 Warsaw, Poland

ENGINEERING STATE-INSENSITIVE OPTICAL LATTICES FOR NARROW MOLECULAR TRANSITIONS

An optical lattice trap contributes no light shift or inhomogeneous broadening if the polarizabilties of the initial and final states for a transition are equal, $\alpha' = \alpha$. In our measurements, we engineer such state-insensitive ("magic") lattices for particular transitions by experimentally controlling both polarizabilities.

For states with total spin quantum number J and azimuthal quantum number m trapped by a linearly polarized lattice, the electric-dipole polarizability has the form [1]

$$\alpha = \alpha_0(\lambda) + \alpha_2(\lambda) \left(\frac{3\cos^2\theta - 1}{2} \right) \left(\frac{3m^2 - J(J+1)}{J(2J-1)} \right). \tag{1}$$

Equation (1) emphasizes three experimentally accessible parameters: (i) the wavelength λ of the lattice light, (ii) the angle θ of tilt between the directions of linear polarization for the lattice and of the quantization axis for the state, and (iii) the choice of sublevel m. For $\theta = 0$, it is equal to the standard "J representation" in terms of the scalar and tensor polarizabilities α_0 and α_2, respectively [2]. Note that $\alpha_2 = 0$ if $J < 1$.

We experimentally control the angle θ for excited-state Sr_2 molecules by applying a magnetic field B_z along the z-axis, perpendicular to the tight-trapping x-axis. This field defines the quantization axis through the linear Zeeman interaction. The angle θ is then set by a rotatable linear polarizer that controls the direction of the lattice polarization, which lies in the yz-plane.
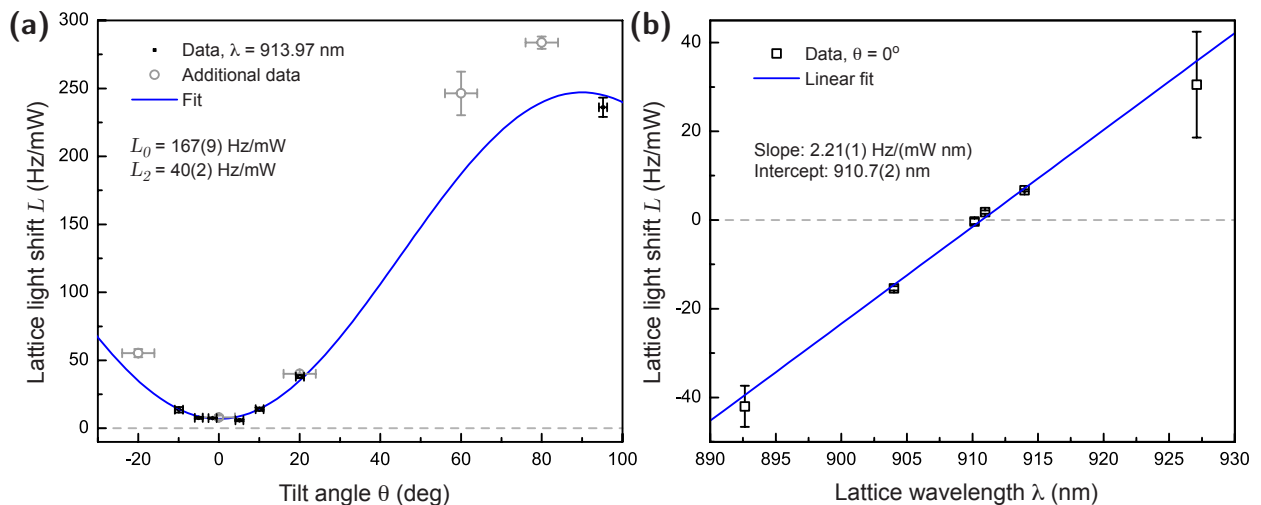

FIG. S1: **Polarization and wavelength tuning of the lattice light shift.** The probed transition is from $v = -2$, $J = 0$, $m = 0$ of $X^1\Sigma_g^+$ to $v' = -4$, $J' = 1$, $m' = 0$ of 1_g. **a,** The shift is controlled by varying the lattice polarization direction relative to the quantum axis. **b,** The shift is controlled by varying the lattice wavelength, at the optimal polarization determined from part (a). The vertical error bars are standard errors from least-squares fitting of the slope L of Eq. (2). The horizontal error bars are instrumental uncertainties in setting the tilt angle. The uncertainties in parenthesis for fit parameters shown are standard errors from least-squares fitting.

For transitions from a $J = 0$ ground state to an excited state with J', we may use Eq. (1) to introduce a lattice

light-shift coefficient

$$L = \frac{1}{\hbar}\frac{\partial \Delta_{\mathrm{AC}}}{\partial P} = L_0(\lambda) + L_2(\lambda)\left[3\cos^2\theta - 1\right]\left[3(m')^2 - J'(J'+1)\right], \tag{2}$$

where Δ_{AC} is the differential AC Stark shift, P is the lattice light power, and the coefficients L_0 and L_2 depend on the choice of states. This form highlights the experimental control of lattice light shifts. To engineer a magic lattice for the transition, it is sufficient to select m', θ, and λ such that $L = 0$. A typical approach is sketched in Fig. S1. After choosing m', the tilt angle θ is adjusted to minimize L, and the wavelength λ is adjusted until $L = 0$. A similar approach was used to engineer a magic lattice for the $^1S_0$–$^3P_1$ E1 transition of ^{88}Sr [3], for which $\theta = \pi/2$ and $\lambda = 914(1)$ nm. For M1 transitions to 1_g states with $J' = 1$, we engineered magic lattices for $m' = 0$ with $\theta = 0$ and λ a few nm below 914 nm. For E1 transitions to 0_u^+ and 1_u states with $J' = 1$, we engineered nearly magic lattices for $m' = 0$ with $\theta = \pi/2$ but with λ within 30 nm of the magic wavelength, because of laser limitations. In this case, $|\alpha'/\alpha - 1| \lesssim 3\%$. For the narrowest E2 transition to a 1_g state with $J' = 2$, we engineered a nearly magic lattice for $m' = \pm 2$ and $\theta = 0$.

AC Stark shifts also contribute to inhomogeneous broadening of spectra in the optical lattice. This broadening was estimated from measurements of the lattice light shift as $\partial\Gamma_{\mathrm{lat}}/\partial P \approx 0.3|L|$ for our nearly magic lattice, where Γ_{lat} is the lattice contribution to the linewidth of a transition. The factor of ~ 0.3 comes from measurements of narrow transitions where the lattice uncertainty dominates the observed width [4].

TRANSITION STRENGTH MEASUREMENTS AND CALCULATIONS

We measure a signal S that is proportional to the number n_J of ground-state Sr_2 ($v = -1$ or -2; $J = 0$ or 2) within a sampled volume of the optical lattice. Prior to measurement, we apply a laser pulse with duration τ and power P along the lattice axis. Depending on the laser-frequency detuning from resonance, δ, this laser pulse may induce absorption for a particular Sr_2 transition. Our goal is to extract the strength of the transition probed by the laser pulse by analyzing $S(\delta)$, which is roughly a Lorentzian dip with a constant background.

We perform transition strength measurements from $J = 0$ such that there is a unique sublevel $m = 0$, but the procedure described below also applies to $J = 2$. During the laser pulse, the ground-state population $n_0(t)$ evolves as

$$\frac{d}{dt}n_0(t) = -\Gamma_0(\delta)n_0(t), \tag{3}$$

where $\Gamma_0(\delta)$ is the absorption rate per molecule. After a pulse of duration τ, the population is

$$n_0(\tau) = n_0(0)\exp[-\Gamma_0(\delta)\tau]. \tag{4}$$

The measured signal is $S_0(\delta) \propto n_0(\tau)$, which far off-resonance we can denote with the shorthand $S_0(\infty) \propto n_0(0)$, such that

$$\frac{S_0(\delta)}{S_0(\infty)} = \exp[-\Gamma_0(\delta)\tau]. \tag{5}$$

We represent the transition strength by the quantity

$$Q = -\frac{1}{\tau P}\int \ln\left[\frac{S_0(\delta)}{S_0(\infty)}\right]d\delta = \frac{1}{P}\int\Gamma_0(\delta)d\delta, \tag{6}$$

because it is proportional to both an Einstein B coefficient and an absorption oscillator strength as explained below. No adjustments are made to account for the quantum numbers m, J, m', or J' in computing Q. In practice, we find Q by fitting a plot of $\ln S_0(\delta)$ with a Lorentzian of area A, which then gives $Q = A/(\tau P)$. The default experimental units are $\mathrm{MHz}/(\mathrm{ms}\cdot\mu\mathrm{W})$. For both E1 and M1 transitions the area under one peak ($J = 0, m = 0$ to $J' = 1, m' = 0$) was calculated. For E2 transitions, the areas under two peaks ($J = 0, m = 0$ to $J' = 2, m' = \pm 1$) were summed. In all cases the probe laser light propagated along the tight-confinement x-axis of the lattice, perpendicular to the quantization z-axis set by an applied magnetic field. For E1 and E2 transitions, the probe light was linearly polarized along $\hat{z}$, and for M1, along $\hat{y}$. Area-preserving broadening mechanisms such as slightly state-sensitive optical lattice or magnetic-field variations do not affect Q, unlike area-changing mechanisms like power broadening. Thus, care was taken to avoid power broadening.

The rate in Eq. (3) is [5]

$$\Gamma_0(\delta) = \frac{W_{12}(\delta)}{N_1} \equiv \frac{1}{N_1} \int w_{12}(\omega)d\omega = B_{12} \int g(\omega)\rho(\omega)d\omega, \tag{7}$$

where W_{12} is an induced absorption rate, N_1 is the number of ground-state molecules, $\rho(\omega)$ is the probe laser energy density per angular frequency at δ, B_{12} is the Einstein B coefficient of induced absorption, and $g(\omega)$ is a normalized lineshape function satisfying $\int g(\omega)d\omega = 1$. For narrow-linewidth lasers, Eq. (7) becomes

$$\Gamma_0(\delta) = B_{12}g(2\pi\delta)I/c, \tag{8}$$

where for a probe beam waist w_0 and electric field amplitude E, the irradiance

$$I = \frac{c\epsilon_0 E^2}{2} = \frac{2P}{\pi w_0^2}. \tag{9}$$

Then

$$\int \Gamma_0(\delta)d\delta = \frac{B_{12}I}{2\pi c}, \tag{10}$$

and the quantity Q we report is

$$Q = \left(\frac{1}{c\,\pi^2 w_0^2}\right)B_{12} = \left(\frac{1}{c\,\pi^2 w_0^2}\right)\left(\frac{\pi e^2}{2\epsilon_0 m_e \hbar \omega_{21}}\right)f_{12}, \tag{11}$$

where m_e and e are the mass and charge of an electron and ω_{21} is the resonant angular frequency of the transition, which is nearly the same for all transitions considered. As shown, this quantity is proportional to both B_{12} and the dimensionless absorption oscillator strength f_{12} for the transition under study. The oscillator strength and the associated dipole and quadrupole operators are conventionally defined as in Ref. [6] and references therein. For calculations, the operators are transformed into the molecular body-fixed frame. Figure 1b in the manuscript is a plot of Q values for the various studied transitions, each normalized by the Q for one particular E1 transition.

Alternatively, Q is related to Rabi frequency ω_R as follows. Consider a two-level system $|1\rangle$ and $|2\rangle$ coupled by a time-dependent perturbation

$$\hat{H}_{\text{int}}(t) = \hat{H}_0 \cos(\omega t). \tag{12}$$

For an E1 transition, $\hat{H}_0 = -\hat{\mathbf{d}} \cdot \mathbf{E}_0$, where $\hat{\mathbf{d}}$ is an electric dipole moment operator; for M1, $\hat{H}_0 = -\hat{\boldsymbol{\mu}} \cdot \mathbf{B}_0$, where $\hat{\boldsymbol{\mu}}$ is a magnetic dipole moment operator; for E2, $\hat{H}_0 = -(1/6)\hat{Q}_{ij}\nabla_i E_j$, were $\hat{Q}_{ij}$ is an electric quadrupole moment operator. If the frequency $\omega = \omega_{21}$, then the population oscillates between the levels at the on-resonance Rabi frequency

$$\omega_R = |\langle 1|\hat{H}_0|2\rangle|/\hbar. \tag{13}$$

This Rabi frequency is related to the quantity Q we report as

$$Q = \frac{1}{4}\left(\frac{\omega_R^2}{P}\right) \tag{14}$$

and can be measured via Rabi oscillations. Equation (14) follows from Eqs. (9, 10, 11) and $\int \Gamma_0(\delta)d\delta = (1/N_1)\int W_{12}(\delta)d\delta = (1/N_1)W_{12}(\omega_{21})\Gamma/4 = \omega_R^2/4$, where Γ is the transition linewidth, the last two steps follow Chs. 4 & 5 of Ref. [7], and we assumed a Lorentzian form of $W_{12}(\delta)$ and a narrow-linewidth laser. Alternatively, Eq. (14) may be derived for E1 transitions as in Ref. [5]. Note that the factor of 1/4 depends on the conventions used to define w_0 and P. We confirmed this relationship for the M1 strengths that are plotted in Fig. 1b of the manuscript.

In calculations of oscillator strengths and radiative decay rates, we employed the following asymptotic forms for the non-vanishing components of the M1 and E2 transition moments between the $X^1\Sigma_g^+$ and 1_g electronic states [8],

$$\langle X^1\Sigma_g^+|\hat{\mu}_{x/y}|1_g\rangle \approx \frac{\mu_B}{\sqrt{2}\hbar}R\langle^1 S_0|\hat{p}_{x/y}|^3 P_1\rangle, \tag{15}$$

$$\langle X^1\Sigma_g^+|\hat{Q}_{xz/yz}|1_g\rangle \approx \frac{1}{\sqrt{2}}R\langle^1 S_0|\hat{r}_{x/y}|^3 P_1\rangle. \tag{16}$$

The growth of these transition moments with the bond length R is explicit in Eqs. (15,16). Note that for E1 transitions to the 1_u and 0_u^+ states, the long-range moment is constant with R,

$$\langle X^1\Sigma_g^+|\hat{\mathbf{r}}|1_u/0_u^+\rangle \approx \sqrt{2}\langle^1 S_0|\hat{\mathbf{r}}|^3 P_1\rangle. \tag{17}$$

CALCULATIONS OF PREDISSOCIATIVE CONTRIBUTIONS TO SUBRADIANT STATE LIFETIMES

The main mechanism responsible for the finite lifetimes of the 1_g states is nonradiative decay (predissociation). The predissociation takes place via nonadiabatic coupling with states of the 0_g^- electronic potential which correlates with the $^1S_0 + {}^3P_0$ asymptote. The coupling Hamiltonian is of the form

$$\widehat{H}_R = -\frac{\hbar^2}{2\mu R^2}(\hat{J}_+\hat{j}_- + \hat{J}_-\hat{j}_+), \qquad (18)$$

where $\hat{j} = \hat{L} + \hat{S}$, and $\hat{J}$, $\hat{j}$, $\widehat{L}$ and $\hat{S}$ are the operators for the total angular momentum, total electronic angular momentum, and electronic orbital and spin angular momenta, respectively.
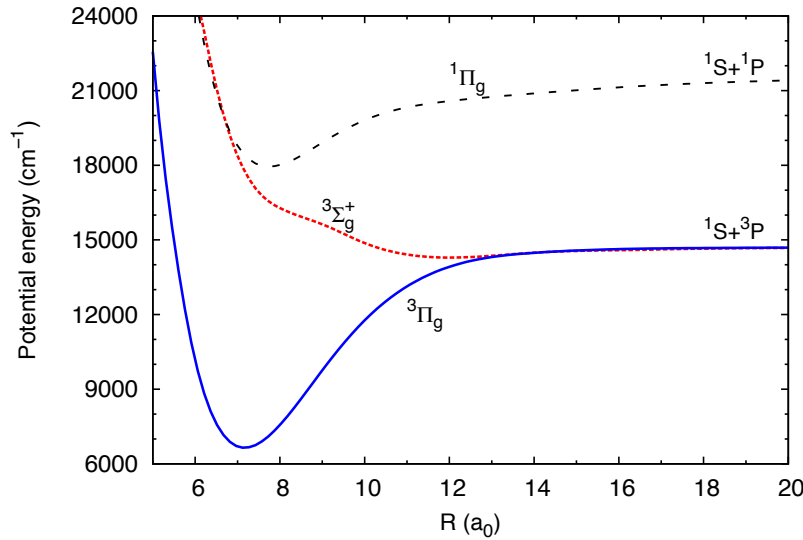

FIG. S2: **Potential energy curves for the $^3\Sigma_g^+$, $^3\Pi_g$, and $^1\Pi_g$ states of Sr$_2$.** This Hund's case (a) picture is helpful for analyzing short-range behavior.

Predissociation widths were calculated from the Fermi golden rule,

$$\Gamma_{pre} = \frac{2\pi}{\hbar}|\langle 1_g, v', J', m'|\widehat{H}_R|0_g^-, E, J', m'\rangle|^2, \qquad (19)$$

where $|0_g^-, E, J', m'\rangle$ is the energy-normalized continuum wavefunction with energy E matching that of the bound level v'. We study subradiant states just below the atomic threshold, so it is reasonable to first analyze the asymptotic behavior of the coupling via $\widehat{H}_R$. The nonadiabatic coupling in Eq. (19) vanishes at large interatomic separations because of the different thresholds of the 0_g^- and 1_g electronic potentials, leading to

$$\langle 1_g|\hat{j}_\pm|0_g^-\rangle \approx \langle {}^3P_1|\hat{j}_\pm|{}^3P_0\rangle = 0. \qquad (20)$$

However, the nonadiabatic coupling does not vanish at short interatomic separations. To analyze the short-range behavior, it is convenient to use the Hund's case (a) basis rather than (c). In this picture, the 1_g state is mainly a mixture of $^3\Pi_g$ and $^3\Sigma_g^+$ electronic states, with a small contribution from $^1\Pi_g$. The 0_g^- state is comprised of the $^3\Pi_g$ and $^3\Sigma_g^+$ states. At short range, $^3\Sigma_g^+$ is strongly repulsive and the $^3\Pi_g$ component dominates, as shown in Fig. S2. Thus the nonadiabatic coupling from Eqs. (18, 19) will be dominated by the following Coriolis interaction involving the $^3\Pi_g$ electronic components,

$$\langle 1_g, v', J', m'|\widehat{H}_R|0_g^-, E, J', m'\rangle \approx -\langle {}^3\Pi_{g,|\Omega|=1}, v', J', m'|\frac{\hbar^2}{2\mu R^2}\left[\hat{J}_+\hat{S}_- + \hat{J}_-\hat{S}_+\right]|{}^3\Pi_{g,|\Omega|=0}, E, J', m'\rangle. \qquad (21)$$

The explicit proportionality to R^{-2} in Eq. (21) disappears after integration over the spatial coordinate, while the integral over the electronic spin and rotational degrees of freedom can be evaluated analytically,

$$\langle {}^3\Pi_{g,|\Omega|=1}, J', m'|\hat{J}_+\hat{S}_- + \hat{J}_-\hat{S}_+|{}^3\Pi_{g,|\Omega|=0}, J', m'\rangle = \sqrt{2J'(J'+1)}. \qquad (22)$$

We have calculated predissociation rates for weakly bound subradiant states with $J' = 1$ and $J' = 3$, assuming Eq. (21) and that the Coriolis coupling is only relevant at short interatomic distances where the $^3\Pi_g$ and $^3\Sigma_g^+$ potentials are significantly different. Due to the strong oscillating character of rovibrational wavefunctions at short range, the calculations of matrix elements in Eq. (19) are difficult to converge. The main contribution to this integral comes from the range near the inner turning points of the rovibrational wavefunctions. To accurately reproduce the experimental linewidths without any modification of the Sr_2 potentials, we require a better knowledge of the short-range potentials than is currently available. Therefore, to improve agreement of the theoretical and experimental linewidths for the 1_g $J' = 1$ levels, we scaled the $^3\Pi_g$ ab initio potential by 1.2%.

While it is challenging to obtain accurate ab initio values of the predisociation linewidths, we can readily reproduce the width ratios for weakly bound levels by using concepts from quantum defect theory to account for short-range effects. A rovibrational wavefunction can be represented as [9]

$$\psi_v(R) = \left(\frac{\partial E_v}{\partial v}\right)_{E=E_v}^{1/2} \left(\frac{2\mu}{\pi\hbar^2}\right)^{1/2} \alpha_v(R, k) \sin(\beta_v(R, k)), \qquad (23)$$

where $\frac{\partial E_v}{\partial v}$ is the vibrational spacing (alternatively, $\frac{\partial v}{\partial E_v}$ is the density of states per unit energy), and $\alpha_v(R, k)$ and $\beta_v(R, k)$ are the quantum amplitude and phase of the state v. The $\alpha_v(R, k)$ and $\beta_v(R, k)$ functions depend on the local wavenumber $k(R) = \sqrt{2[E_v - V(R)]\mu}/\hbar$. For different weakly bound levels, $\alpha_v(R, k)$ and $\beta_v(R, k)$ are nearly the same at short range, so the $\Psi_{v'}$ wavefunctions differ only due to their local vibrational spacing. The wavefunctions $|0_g^-, E, J', m'\rangle$ are nearly identical for all v' due to the large scattering energy E. Thus, the matrix elements $\Gamma_{\text{pre}}(v', J')$ from Eq. (19) differ only due to the vibrational spacing factor. Therefore, the predissociation rates can be written as

$$\Gamma_{\text{pre}}(v) = p\left(\frac{\partial E_v}{\partial v}\right)_{E=E_v}, \qquad (24)$$

where the primes were dropped, and p is the only free parameter quantifying the overlap between the scattering and bound rovibrational wavefunctions.

We can calculate $\frac{\partial E_v}{\partial v}$ by numerical differentiation of the measured bound energies, and then fit the single parameter p to the measured widths as plotted in Fig. 3 of the manusript. The linear dependence of the width on the vibrational spacing near the asymptote, predicted in Ref. [10], is thus confirmed. From the LeRoy-Bernstein formula [11] we can relate the vibrational spacing near the asymptote to the bond length by assuming interatomic interaction of the form C_n/R^n,

$$\frac{\partial E_v}{\partial v} \propto E_v^{\frac{n+2}{2n}} \propto R^{-\frac{n+2}{2}}. \qquad (25)$$

Thus the predissociation rate should scale $\propto 1/R^{2.5}$ for the C_3/R^3 interaction and $\propto 1/R^4$ for the C_6/R^6 interaction. For the Sr_2 1_g state, the C_3-C_6 crossover occurs near $v' = -2$, and our predissociation measurements are directly sensitive to it.

ZEEMAN EFFECT IN SUBRADIANT STATES

We have measured and calculated the linear and quadratic Zeeman-shift coefficients of the least-bound subradiant 1_g states with $J' = 1, 3$. The results are shown in Table S1. We parameterize linear and higher-order Zeeman shifts as [12]

$$\Delta E_b \approx g\mu_B m'B + \bar{q}\mu_B B^2 \qquad (26)$$

over a range of ± 2 G of the magnetic field B, where $\bar{q} = \bar{q}(v', J', m')$ depend on m' while $g = g(v', J')$ do not. Note that as defined, the binding energies are negative, so that positive shifts make molecules less bound. For ideal Hund's case (c) 1_g states at the intercombination-line asymptote, the linear shifts [12] should have $g \approx (g_{\text{atomic}})/[J'(J' + 1)] = 3/4, 1/8$ for $J' = 1, 3$.

Comparison between the predicted and measured coefficients shows excellent agreement. Zeeman shift measurements are critical for refining the molecular model, since the linear coefficients constrain nonadiabatic Coriolis mixing between molecular states and the quadratic coefficients are highly sensitive to binding energies. Table S1 reveals nearly ideal Hund's case (c) shifts for $J' = 1$, while for $J' = 2$ the nonadiabatic contributions are large. This may be

J'	v'	E_{th}	E_{exp}	g_{th}	g_{exp}	$|m'|$	$\bar{q}_{th}$	$\bar{q}_{exp}$
1	-1	19.3	19.0420(38)	0.750	0.749(1)	0	-0.0865	-0.086(2)
						1	-0.0465	-0.046(2)
1	-2	315	316(1)	0.750	0.744(2)	0	-0.0189	-0.0192(3)
						1	-0.0112	-0.014(2)
1	-3	1651	1669(1)	0.750	0.747(1)	0	-0.00815	-0.00817(6)
						1	-0.00543	-0.0062(4)
1	-4	5057	5168(1)	0.750	0.747(1)	0	-0.00543	-0.00547(4)
						1	-0.00364	-0.00472(5)
2	-1	7.2	7(1)	0.429	0.426(1)	0	0.0288	0.030(1)
						1	0.0112	0.014(1)
						2	-0.0404	-0.039(2)
2	-2	266	270(1)	0.347	0.3480(4)	0	0.00736	0.0102(1)
						1	0.00364	0.004(1)
						2	-0.00729	-0.009(1)
2	-3	1536	1581(1)	0.312	0.308(2)	0	0.00307	
						1	0.00157	0.001(5)
						2	-0.00300	-0.001(2)
2	-4	4866	5035(1)	0.304	0.293(1)	0	0.0193	
						1	0.00093	-0.001(1)
						2	-0.00214	-0.004(1)
3	-1	185	193(1)	0.125				
3	-2	1401	1438(1)	0.125				
3	-3	4684	4826(1)	0.125				

TABLE S1: **Predicted and measured Zeeman shifts for 1_g subradiant states of Sr$_2$.** Coefficients up to the second order are included. The binding energies E are in MHz, the linear g-factors are unitless, and the quadratic shift coefficients $\bar{q}$ are in G^{-1}. The g and q uncertainties are standard errors from least-squares fitting of spectroscopic peak positions versus magnetic field, and include the estimated inaccuracy of the applied magnetic field. The value and uncertainty for the $v' = -1$, $J' = 1$ binding energy come from extrapolating a peak-to-shelf frequency difference [12] to zero magnetic field and probe and lattice light powers.

explained by Coriolis mixing of the 1_g potential with 0_g^+ (Fig. 3a in the manuscript). Such mixing is not possible for odd J', since in Sr$_2$ molecules the permutational symmetry permits only even-J' levels for the 0_g^+ potential.

---

* Present address: Institute of Physics, University of Kassel, Heinrich-Plett-Strasse 40, 34132 Kassel, Germany

[1] M. Auzinsh, D. Budker, and S. Rochester, *Optically Polarized Atoms: Understanding light-atom interactions* (Oxford University Press, Oxford, 2010).

[2] J. Mitroy, M. S. Safronova, and C. W. Clark, J. Phys. B **43**, 202001 (2010).

[3] T. Ido and H. Katori, Phys. Rev. Lett. **91**, 053001 (2003).

[4] M. McDonald, B. H. McGuyer, G. Z. Iwata, and T. Zelevinsky, arXiv:1409.5852 (2014).

[5] R. C. Hilborn, Am. J. Phys. **50**, 982 (1982).

[6] S. Tojo and M. Hasuo, Phys. Rev. A **71**, 012508 (2005).

[7] A. E. Siegman, *Lasers* (University Science Books, California, 1986).

[8] B. Bussery-Honvault and R. Moszynski, Mol. Phys. **104**, 2387 (2006).

[9] F. H. Mies, J. Chem. Phys. **80**, 2514 (1984).

[10] F. H. Mies and P. S. Julienne, J. Chem. Phys. **80**, 2526 (1984).

[11] R. J. LeRoy and R. B. Bernstein, J. Chem. Phys. **52**, 3869 (1970).

[12] B. H. McGuyer, C. B. Osborn, M. McDonald, G. Reinaudi, W. Skomorowski, R. Moszynski, and T. Zelevinsky, Phys. Rev. Lett. **111**, 243003 (2013).